J Arid Land (2024) 16(1): 91–109
https://doi.org/10.1007/s40333-024-0051-x

Science Press Springer-Verlag

Spatiotemporal characteristics and driving mechanisms of land use/land cover (LULC) changes in the Jinghe River Basin, China

WANG Yinping[1], JIANG Rengui[1*], YANG Mingxiang[2], XIE Jiancang[1], ZHAO Yong[2], LI Fawen[3], LU Xixi[4]

[1] State Key Laboratory of Eco-hydraulics in Northwest Arid Region of China, Xi'an University of Technology, Xi'an 710048, China;
[2] State Key Laboratory of Simulation and Regulation of Water Cycle in River Basin, China Institute of Water Resources and Hydropower Research, Beijing 100038, China;
[3] State Key Laboratory of Hydraulic Engineering Simulation and Safety, Tianjin University, Tianjin 300072, China;
[4] Department of Geography, National University of Singapore, Singapore 117570, Singapore

Abstract: Understanding the trajectories and driving mechanisms behind land use/land cover (LULC) changes is essential for effective watershed planning and management. This study quantified the net change, exchange, total change, and transfer rate of LULC in the Jinghe River Basin (JRB), China using LULC data from 2000 to 2020. Through trajectory analysis, knowledge maps, chord diagrams, and standard deviation ellipse method, we examined the spatiotemporal characteristics of LULC changes. We further established an index system encompassing natural factors (digital elevation model (DEM), slope, aspect, and curvature), socio-economic factors (gross domestic product (GDP) and population), and accessibility factors (distance from railways, distance from highways, distance from water, and distance from residents) to investigate the driving mechanisms of LULC changes using factor detector and interaction detector in the geographical detector (Geodetector). The key findings indicate that from 2000 to 2020, the JRB experienced significant LULC changes, particularly for farmland, forest, and grassland. During the study period, LULC change trajectories were categorized into stable, early-stage, late-stage, repeated, and continuous change types. Besides the stable change type, the late-stage change type predominated the LULC change trajectories, comprising 83.31% of the total change area. The period 2010–2020 witnessed more active LULC changes compared to the period 2000–2010. The LULC changes exhibited a discrete spatial expansion trend during 2000–2020, predominantly extending from southeast to northwest of the JRB. Influential driving factors on LULC changes included slope, GDP, and distance from highways. The interaction detection results imply either bilinear or nonlinear enhancement for any two driving factors impacting the LULC changes from 2000 to 2020. This comprehensive understanding of the spatiotemporal characteristics and driving mechanisms of LULC changes offers valuable insights for the planning and sustainable management of LULC in the JRB.

Keywords: land use/land cover (LULC) changes; driving mechanisms; trajectory analysis; geographical detector (Geodetector); Grain for Green Project; Jinghe River Basin

Citation: WANG Yinping, JIANG Rengui, YANG Mingxiang, XIE Jiancang, ZHAO Yong, LI Fawen, LU Xixi. 2024. Spatiotemporal characteristics and driving mechanisms of land use/land cover (LULC) changes in the Jinghe River Basin, China. Journal of Arid Land, 16(1): 91–109. https://doi.org/10.1007/s40333-024-0051-x

*Corresponding author: JIANG Rengui (E-mail: jrengui@163.com)
Received 2023-08-15; revised 2023-12-01; accepted 2023-12-04

1 Introduction

Land use/land cover (LULC) serves as a critical indicator of the intricate interplay between human society and the natural environment (Luo et al., 2022; Yang et al., 2022). LULC changes, largely driven by human activities, are a key component of global environmental change and a significant reflection of human impacts on the environment (Wang et al., 2012). In recent decades, human actions and policies have altered LULC, triggering various challenges for climate, biodiversity, ecosystems, hydrology, food security, and socio-economics, with notable effects including urban expansion, wetland conversion, and deforestation (Zhai et al., 2021; He et al., 2022). Understanding the spatial and temporal dynamics of LULC changes is vital for sustainable land management, contributing significantly to both sustainable development and ecological equilibrium (Yang et al., 2021). The complexity and uncertainty of LULC change processes have positioned this subject as a research focal point, considering the ecological and environmental impacts. Extensive studies on LULC changes have primarily examined the spatiotemporal characteristics, driving factors, and future projections through modeling (Ji et al., 2023; Schirpke et al., 2023).

Past research on LULC changes has encompassed the detection of changes, identification of change nature, quantification of the area affected, and evaluation of spatial patterns (Zhou et al., 2008; Kayitesi et al., 2022). Methods such as transfer matrix, intensity analysis, and change trajectory analysis have been applied to study LULC change processes (Xia et al., 2023). While the transfer matrix and intensity analysis focus on two specific time points, the change trajectory analysis extends to multiple time points (Liu et al., 2022). For example, Liu et al. (2022) employed these methods to assess changes in ecology-production-living land within the Wujiang River Basin, China. The change trajectory analysis method, in particular, has proven effective in elucidating the nuances of LULC change processes (Gong et al., 2022; Li et al., 2022). Zomlot et al. (2017) integrated hydrological modeling with spatiotemporal LULC trajectories to quantify the influence of LULC changes on groundwater recharge. Similarly, Wang et al. (2019a) used LULC change trajectories to explore the impact of urban expansion on urban ecological environment.

Based on the spatiotemporal characteristics of LULC changes, past research has differentiated between proximate causes and underlying driving forces (Heidarlou et al., 2020). Proximate causes refer to immediate human activities at specific locations, while underlying driving forces encompass broader social processes such as demographic, economic, technological, institutional, sociocultural, and locational factors. Studies have indicated that LULC changes result from the interplay of natural environment and socio-economic factors (e.g., Zhao et al., 2018). Accurate identification of LULC change drivers requires a comprehensive consideration of these aspects (Chen et al., 2021). The driving impacts can be categorized into single and interactive effects, acknowledging the spatiotemporal heterogeneity of these influences on LULC changes. Previous studies have utilized the geographical detector (Geodetector) to analyze the driving factors under various contexts, such as urbanization (Xu and Hou, 2019), wetland conversion (Zhang et al., 2021), cultivated land use efficiency (Zhou et al., 2022), desertification (Han et al., 2021), and non-grain producing areas (Zhu et al., 2022).

Since the implementation of the "Grain for Green Project" in China in 1999, the Jinghe River Basin (JRB) has experienced large-scale revegetation. Current studies on LULC changes in the JRB have primarily focused on the spatiotemporal characteristics and driving mechanisms of the Normalized Difference Vegetation Index (NDVI) or specific land use types (Huang et al., 2021; Xu et al., 2022a). While these studies have considered the impact of single factors, they often overlooked the combined influence and interaction between factors. Thus, this paper examines both the temporal and spatial characteristics of LULC changes in the JRB, as well as the combined effect of various driving factors on these changes. The paper aims to explore the spatiotemporal characteristics of LULC changes from 2000 to 2020 in the JRB, and ascertain the driving mechanisms behind these changes. Specifically, we seek to answer the following two questions: (1) What are the spatiotemporal characteristics of LULC changes in the JRB during the

period 2000–2020? (2) How do driving factors and their interactions influence the LULC changes, and what are the underlying mechanisms? The findings will elucidate the driving mechanisms of LULC changes in the JRB more clearly, offering a scientific basis for more effective LULC management in a changing environment.

2 Materials and methods

2.1 Study area

The JRB, a significant secondary tributary of the Yellow River Basin and the largest tributary of the Weihe River Basin, extends over Shaanxi Province, Gansu Province, and Ningxia Hui Autonomous Region in China. It spans a total length of 455.10 km and covers an area of 45,421 km^2 (Jiang et al., 2019; Wang et al., 2022), as depicted in Figure 1. Characterized by a typical temperate continental climate, the JRB lies in a transitional zone between semi-arid and semi-humid climates. From 1960 to 2019, the mean annual precipitation was approximately 295.39–741.06 mm, and the mean annual temperature was around 6.88℃–11.86℃. The predominant LULC types in the JRB are farmland, grassland, and forest, collectively comprising over 80% of the total area (Xu et al., 2022b).

The implementation of the "Grain for Green Project" in 1999 marked a significant shift in the LULC of the JRB. Post-project studies (e.g., Yu et al., 2023) have identified a decrease in the annual runoff in the JRB, attributed primarily to natural vegetation changes. Furthermore, research has indicated that LULC changes critically impact the river health in the JRB, which is currently classified as being at a sick level (Wang et al., 2019b). These changes also significantly influence the ecosystem pattern and are a key driver of ecosystem services (Wang et al., 2019c; Xu et al., 2022b). Therefore, understanding the spatiotemporal characteristics and driving mechanisms of LULC changes is crucial for supporting ecological protection and promoting sustainable LULC development in the JRB.

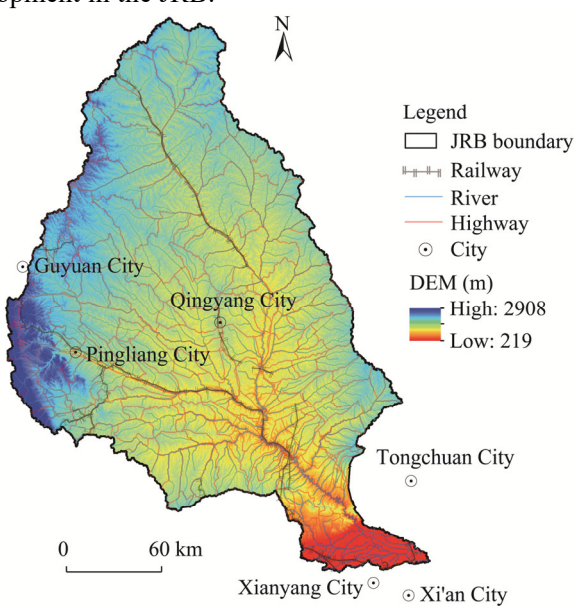

Fig. 1 Overview of the Jinghe River Basin (JRB) and the spatial distribution of railways, rivers, and highways in the JRB. DEM, digital elevation model. The data on railways, rivers, and highways were sourced from the National Catalogue Service for Geographic Information (https://www.webmap.cn/).

2.2 Data sources

2.2.1 Land use data

The land use data for this study were sourced from the GlobeLand30 (https://www.webmap.cn/mapDataAction.do?method=globalLandCover), by utilizing a methodology that combines pixel-

and object-based approaches with knowledge and offers a spatial resolution of 30 m. The overall classification accuracy for various regions exceeds 80%, ensuring a reliable quality assessment (Helbich et al., 2019). This dataset encompasses ten primary LULC types: farmland, forest, grassland, shrubland, wetland, water, tundra, artificial surfaces, bareland, and permanent snow and ice. Within the JRB, the relevant LULC types include farmland, forest, grassland, shrubland, wetland, water, artificial surfaces, and bareland. Following the reclassification standards from existing literature (Dong et al., 2020), we reclassified these LULC types into six categories: farmland, forest (including forest and shrubland of primary LULC types), grassland, urban land (artificial surfaces), water body (comprising wetland and water), and bareland. Figure 2 illustrates the spatial distribution of reclassified LULC types in the JRB for the years 2000, 2010, and 2020.

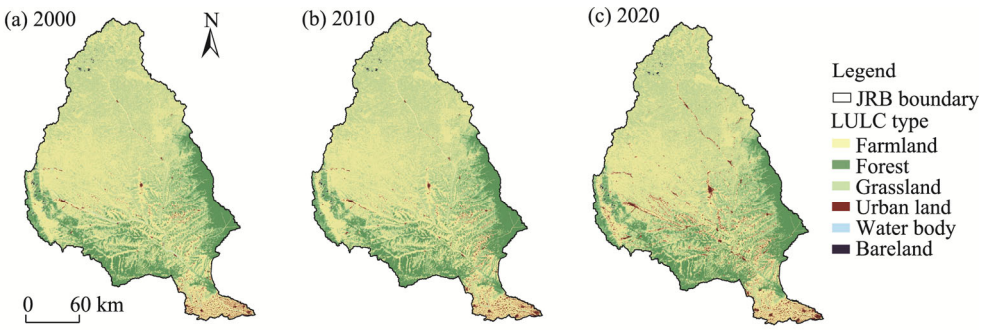

Fig. 2 Spatial distribution of reclassified land use/land cover (LULC) types in 2000 (a), 2010 (b), and 2020 (c) in the JRB

2.2.2 Driving factors

For analyzing the driving factors influencing LULC changes in the JRB, we considered several factors that are both quantifiable and accessible. These factors were categorized into natural, socio-economic, and accessibility factors. Table 1 lists the selected ten driving factors along with their respective data sources.

Table 1 Driving factors of land use/land cover (LULC) changes selected in the study and their data sources

Category	Factor	Unit	Time period	Data source
Natural factors	DEM	m	2019	Geospatial Data Cloud (https://www.gscloud.cn/)
	Slope	-	2019	Calculated based on DEM
	Aspect	-	2019	
	Curvature	-	2019	
Socio-economic factors	GDP	10^4 CNY/km^2	2005 and 2015	Resource and Environment Science and Data Center (https://www.resdc.cn/)
	Population	10^4 persons/km^2	2005 and 2015	
Accessibility factors	Distance from railways	km	2015	National Catalogue Service for Geographic Information (https://www.webmap.cn/)
	Distance from highways	km	2015	
	Distance from water	km	2015	
	Distance from residents	km	2015	

Note: DEM, digital elevation model; GDP, gross domestic product. "-" denotes dimensionless.

It should be noted that for natural factors, a discussion of climate factors is omitted from this study because a separate analysis of their effects is forthcoming in subsequent studies. In high-elevation areas, farmland is generally less prevalent. Factors like slope and curvature are associated with geological hazards such as landslides and debris flows, while aspect influences plant growth. On the socio-economic front, changes in GDP reflect national economic

development, and population changes indicate regional demographic trends, indirectly signifying economic growth. In terms of accessibility factors, the distances from railways, highways, water, and residents all affect the distribution of LULC types. Resampled raster data of all driving factors with a resolution of 30 m×30 m are presented in Figure 3.

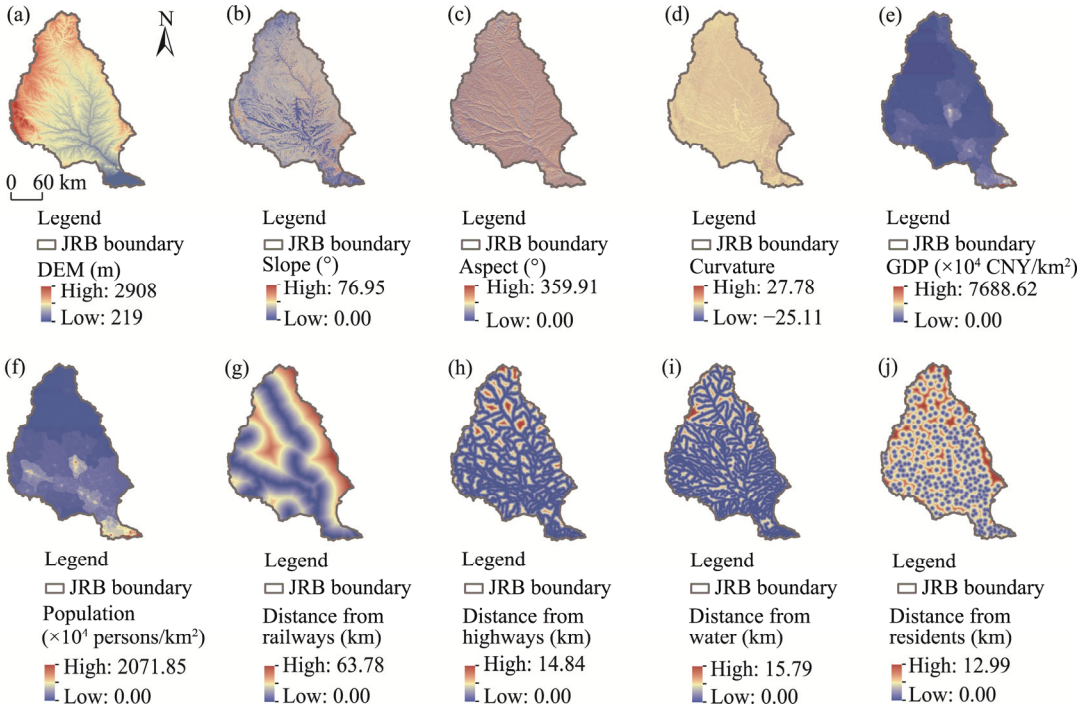

Fig. 3 Spatial distribution of driving factors including DEM (a), slope (b), aspect (c), and curvature (d) in 2019, and GDP (e), population (f), distance from railways (g), distance from highways (h), distance from water (i), and distance from residents (j) in 2015 in the JRB. GDP, gross domestic product.

2.3 Methods

2.3.1 Trajectory analysis method

In this study, numbers 1–6 were used to represent the six LULC types (corresponding to farmland, forest, grassland, urban land, water body, and bareland, respectively), quantifying LULC change trajectories to illustrate the dynamic changes in the JRB at different time nodes in a continuous time series. The change trajectory code for each grid was computed using the following formula (Wang et al., 2012):

$$\mathrm{LCTC} = T_1 \times 10^{n-1} + T_2 \times 10^{n-2} + \cdots + T_i \times 10^{n-i} + \cdots + T_n, \quad (1)$$

where LCTC represents the LULC change trajectory code of each grid within a specific time interval; T_i is the LULC type code of each grid at time node i; and n is the number of time nodes in that time interval.

At time nodes of 2000, 2010, and 2020, we categorized LULC change trajectories into stable, early-stage, late-stage, repeated, and continuous change types based on the dynamic change processes from 2000 to 2020 (Niu et al., 2022). The stable change type indicates no change in the LULC category over the three time nodes (e.g., farmland-farmland-farmland). The early-stage change type involves a change between 2000 and 2010 while a stability from 2010 to 2020 (e.g., farmland-forest-forest). The late-stage change type represents a stability between 2000 and 2010, followed by a change from 2010 to 2020 (e.g., farmland-farmland-forest). The repeated change type denotes a change between 2000 and 2010 but a reversion to the original state by 2020 (e.g., farmland-forest-farmland). The continuous change type reflects distinct LULC types at each time node (e.g., farmland-forest-grassland). LCTC of each grid was determined in ArcGIS, facilitating

the quantification of each change type in the study area.

Generally, the net change, exchange, total change, and transfer rate were selected as metrics to describe the quantitative and spatial changes in LULC types (Asenso Barnieh et al., 2022). Net change quantifies the extent of change in a LULC type, while exchange accounts for the spatial change. For instance, a net change of zero in LULC type *a* might result from a 10% conversion from LULC type *a* to type *b*, and a 10% conversion from LULC type *c* to type *a*. Thus, even with a net change of zero, the exchange does not equal to zero.

$$N_a = \left| LP_{aj} - LP_{ai} \right|, \tag{2}$$

$$E_a = 2 \times \min\left(LP_{ai} - LP_{aa}, LP_{aj} - LP_{aa} \right), \tag{3}$$

$$C_a = N_a + E_a, \tag{4}$$

$$R_{ab} = \frac{LP_{ab}}{\sum_{a=1}^{n}\sum_{b=1}^{n} LP_{ab}} \times 100\% \left(a \neq b \right), \tag{5}$$

where N_a (%) represents the net change of LULC type *a*; LP_{ai} (%) and LP_{aj} (%) denote the area percentages of LULC type *a* at the beginning (*i*) and end (*j*) of the study period, respectively; E_a (%) describes the exchange of LULC type *a*; LP_{aa} (%) indicates the area percentage of LULC type *a* that remains unchanged; C_a (%) is the total change of LULC type *a*; R_{ab} (%) represents the transfer rate from LULC type *a* to type *b*; and LP_{ab} (km^2) is the area changing from LULC type *a* to type *b* during the study period. Cumulative transfer rate (%) is the sum total of the transfer rate from LULC type *a* to type *b*.

The LULC knowledge map effectively visualizes changes between two time nodes. Additionally, the chord diagram can be used to depict these changes (Wang et al., 2023). The chord diagram intuitively displays the areas transferred out of and into each LULC type and illustrates the direction of these conversions. The LULC transfer matrix is effectively represented using the chord diagram.

2.3.2 Standard deviation ellipse

The spatial characteristics of LULC changes were analyzed using the spatial center of gravity migration model. By employing the Spatial Statistics tools in ArcGIS, we derived the standard deviation ellipses from geographic element data at two time nodes. This method, introduced by Lefever (1926), is widely used in socio-economic and ecological research (Zhao et al., 2023). The standard deviation ellipse can help capture the spatial change trajectories and distribution characteristics of geographical elements across multiple dimensions. Key parameters, including the center, azimuth angle, and lengths of its long and short axes, quantitatively represent the centrality, distribution range, and directional deviation of geographical elements. The long axis indicates the direction of the LULC change distribution, while the short axis represents its range. The ratio of the short to long axis signifies the spatial shape, and the closer the ratio is to 1.0, the more circular the standard deviation ellipse is, suggesting more dispersed LULC changes with less directional spatial distribution. The difference between the long and short axes reflects the dispersion and cohesion of LULC changes, with a greater difference indicating a stronger cohesion.

$$SDE_X = \sqrt{\frac{\sum_{k=1}^{m}\left(X_k - \overline{X} \right)^2}{m}}, \tag{6}$$

$$SDE_Y = \sqrt{\frac{\sum_{k=1}^{m}\left(Y_k - \overline{Y} \right)^2}{m}}, \tag{7}$$

$$\tan\theta = \frac{\left(\sum_{k=1}^{m}\widetilde{X_k}^2 - \sum_{k=1}^{m}\widetilde{Y_k}^2\right) + \sqrt{\left(\sum_{k=1}^{m}\widetilde{X_k}^2 - \sum_{k=1}^{m}\widetilde{Y_k}^2\right)^2 + 4\left(\sum_{k=1}^{m}\widetilde{X_k}\widetilde{Y_k}\right)^2}}{2\sum_{k=1}^{m}\widetilde{X_k}\widetilde{Y_k}}, \tag{8}$$

$$\sigma_X = \sqrt{2}\sqrt{\frac{\sum_{k=1}^{m}\left(\widetilde{X_k}\cos\theta - \widetilde{Y_k}\cos\theta\right)^2}{m}}, \tag{9}$$

$$\sigma_Y = \sqrt{2}\sqrt{\frac{\sum_{k=1}^{m}\left(\widetilde{X_k}\cos\theta + \widetilde{X_k}\cos\theta\right)^2}{m}}, \tag{10}$$

where SDE_X and SDE_Y represent the spatial coordinates of the mean center of the standard deviation ellipse along the X and Y axes, respectively; m is the number of geographical elements; X_k and Y_k represent the spatial coordinates of each geographical element k along the X and Y axes, respectively; $\overline{X}$ and $\overline{Y}$ are the arithmetic mean centers of X_k and Y_k, respectively; θ (°) is the azimuth angle, which is the direction cosine shift of the standard deviation ellipse; $\widetilde{X_k}$ and $\widetilde{Y_k}$ represent the mean center deviations of X_k and Y_k, respectively; and σ_X and σ_Y are the standard deviations along the X and Y axes, respectively.

2.3.3 Geographical detector (Geodetector) model

The Geodetector model, based on the spatial distribution similarity between independent and dependent variables, is adept at detecting the spatial differentiation to analyze the driving effect of independent variables on dependent ones (Wang et al., 2010). The Geodetector is suitable for both quantitative and qualitative variables, especially type variables, and is particularly effective in driving mechanism analysis of LULC changes. The Geodetector is not affected by the collinearity problem of independent variables, but its use is constrained by the visual basics of applications, with a maximum data line limit of 32,767. The Geodetector encompasses factor detector, interaction detector, risk detector, and ecological detector (Zhou et al., 2018). This study utilized the factor detector and interaction detector to analyze the influence of individual driving factors and their combined effect on LULC changes.

The factor detector employs the q values to measure the extent to which a driving factor explains the spatial differentiation of LULC changes. The q values ranged between 0.000 and 1.000, with higher values indicating a stronger explanatory power of driving factors on LULC changes.

$$q = 1 - \frac{\sum_{s=1}^{L} N_s \sigma_s^2}{N\sigma^2}, \tag{11}$$

where q is the explanatory power of driving factors on the spatial differentiation of LULC changes; s represents the classification number of independent and dependent variables, with s=1, 2, …, L; N_s and N denote the number of units in class s and in the entire region, respectively; and σ_s^2 and σ^2 are the variances of the dependent variables in class s and in the entire region, respectively.

The interaction detector identifies interactions among different driving factors, assessing whether their combined effect increases, weakens, or independently influences the explanation power of LULC changes (Zhan et al., 2018). Its process is to calculate the q values of any two single driving factors and the combined q value of these two driving factors, and then compare thee three q values to deduce different interaction outcomes, as shown in Table 2.

3 Results

3.1 Quantitative characteristics of LULC changes

Figure 4 shows the knowledge maps of LULC changes in the periods 2000–2010 and 2010–2020

Table 2 Judgement criteria and interaction types between any two driving factors on influencing the spatial differentiation of LULC changes

Judgement criteria	Interaction type
$q(x_1 \cap x_2)<\text{Min}(q(x_1), q(x_2))$	Nonlinear weakening
$\text{Min}(q(x_1), q(x_2))<q(x_1 \cap x_2)<\text{Max}(q(x_1), q(x_2))$	Single-factor nonlinear weakening
$q(x_1 \cap x_2)>\text{Max}(q(x_1), q(x_2))$	Bilinear enhancement
$q(x_1 \cap x_2)=q(x_1)+q(x_2)$	Independence
$q(x_1 \cap x_2)>q(x_1)+q(x_2)$	Nonlinear enhancement

Note: x_1 is a driving factor of LULC changes; x_2 is another driving factor of LULC changes; $q(x_1)$ and $q(x_2)$ are the explanatory power values of x_1 and x_2 on LULC changes, respectively; $q(x_1 \cap x_2)$ is the explanatory power of the interaction of x_1 and x_2 on LULC changes. Min, minimum; Max, maximum.

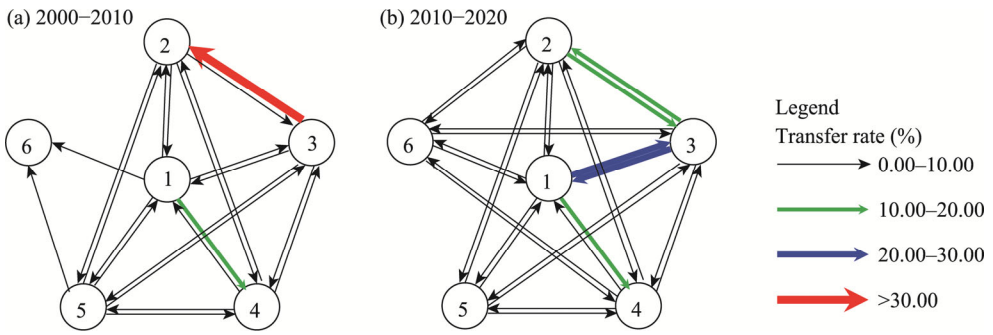

Fig. 4 Knowledge maps of LULC changes in the periods 2000–2010 (a) and 2010–2020 (b) in the JRB. Numbers 1–6 represent farmland, forest, grassland, urban land, water body, and bareland, respectively. The directed arrows signify the conversion directions of LULC changes, the thickness of each line indicates the transfer rate, and the number of lines corresponds to the number of LULC change trajectories.

in the JRB. During 2000–2010, 22 change trajectories were identified (Fig. 4a). The most significant change trajectory was the transfer rate of grassland to forest (35.99%), followed by the conversion of farmland to urban land (14.42%). As depicted in Figure 5, farmland experienced the largest total change (1.32%) during this period (2000–2010). However, this change was predominantly due to exchanges, with a minimal net change of only 0.01%, indicating that the quantitative shift in farmland was relatively insignificant. Conversely, the total changes in forest and grassland were 1.09% and 1.22%, respectively, with their net changes exceeding the exchanges. This suggests that the conversions in forest and grassland during 2000–2010 were more pronounced in terms of quantity.

In the period 2010–2020, there were 28 LULC change trajectories in the JRB (Fig. 4b). The transfer rates of farmland to grassland and grassland to farmland were 22.82% and 24.17%, respectively. Similarly, the transfer rates of forest to grassland and grassland to forest were also significant, with values of 14.01% and 12.68%. According to Figure 5, the net changes in farmland, forest, and grassland (1.05%, 0.03%, and 0.06%, respectively) were lower than their exchanges (7.19%, 4.29%, and 8.60%, respectively), indicating that substantial quantitative conversions among these LULC types were limited. However, the transfer rate of farmland to urban land was notable, at 11.39%. In line with Figure 5, the net change in urban land exceeded the exchange, suggesting that a high transfer rate from farmland and the expansion of urban land was more significant in this period.

Chord diagrams were utilized to illustrate the LULC change trajectories and transfer areas in the periods 2000–2010 and 2010–2020, as depicted in Figure 6. Analysis of Figure 6a reveals that the largest transfer area (both transfer-in area and transfer-out area) from 2000 to 2010 occurred in farmland, amounting to 601.14 km^2, followed by grassland (554.26 km^2) and forest (495.36 km^2). The balance between the transfer-in and transfer-out areas in farmland suggests negligible quantitative change during 2000–2010, aligning with the net change conclusions for farmland

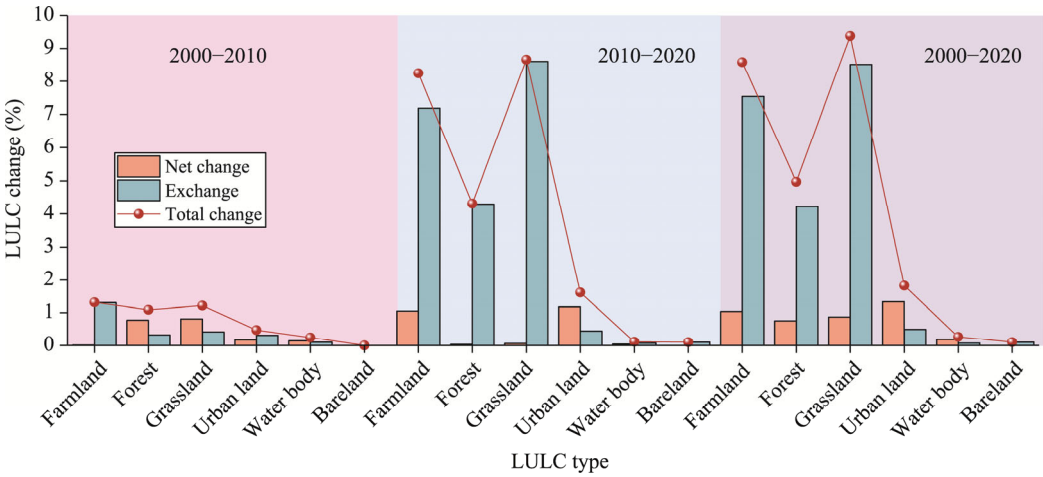

Fig. 5 Variations in the net change, exchange and total change of each LULC type in the periods 2000–2010, 2010–2020, and 2000–2020 in the JRB

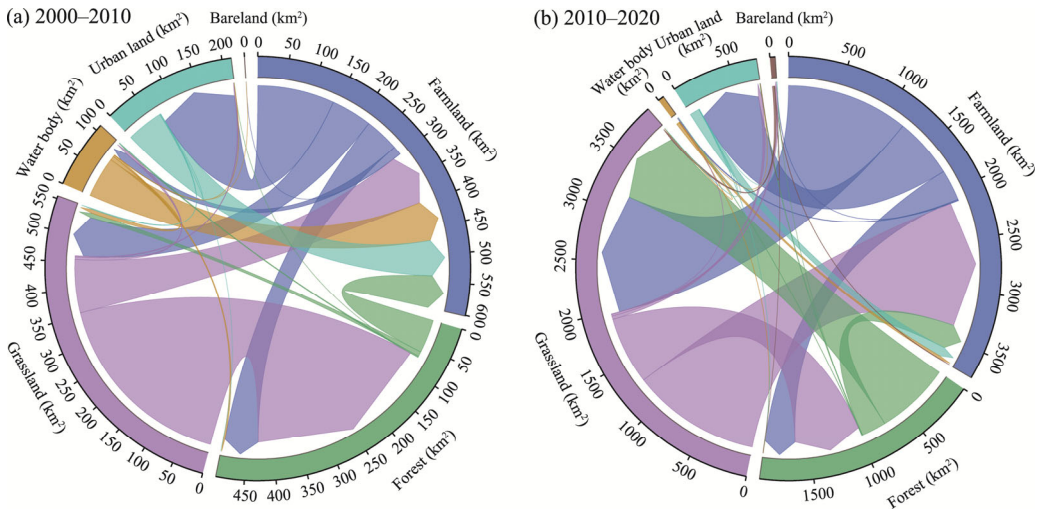

Fig. 6 Chord diagrams showing the LULC change trajectories in the periods 2000–2010 (a) and 2010–2020 (b) in the JRB. In these diagrams, the length of each arc represents the transfer area (both transfer-in area and transfer-out area) of each LULC type. The direction of each arrow indicates the transfer-in direction, while the thickness of each line denotes the magnitude of transfer-in area or transfer-out area.

shown in Figure 5. Notably, the transfer-out area of grassland was substantially larger than its transfer-in area, being 4.93 times larger. Conversely, the transfer-in area of forest significantly exceeded its transfer-out area, being 5.83 times greater. This trend correlates with the predominant conversion of grassland to forest, mirroring the high transfer rate from grassland to forest observed in Figure 4a. For urban land, the transfer-in area predominantly originated from the conversion of farmland to urban land, while the transfer-out area was largely from the conversion of urban land to farmland, confirming the findings in Figure 5 that the exchange of urban land exceeded its net change. Water body exhibited a larger transfer-out area than transfer-in area, primarily transitioning to farmland.

Figure 6b indicates that during 2010–2020, grassland experienced the largest transfer area (3928.20 km^2), followed by farmland (3733.54 km^2) and forest (1953.68 km^2), with increases of 7.09, 6.21, and 3.94 times, respectively, compared to the transfer areas during 2000–2010. The transfer-in area and transfer-out area of grassland and forest were relatively balanced, suggesting no significant quantitative changes in these LULC types, as corroborated by the net change from 2010 to 2020 shown in Figure 5. The transfer-out area of farmland slightly exceeded the

transfer-in area, with respective areas of 2105.08 and 1628.46 km^2. The primary transfer for grassland was the conversion from farmland, while the primary transfer for forest was its conversion to farmland. The main transfer-in source of farmland was grassland, while its primary transfer-out destinations were grassland, urban land, and forest. This aligns with the observed higher transfer rates of farmland to grassland and forest to grassland (Fig. 4b). Urban land again showed a larger transfer-in area than transfer-out area, with the former being 6.35 times larger than the latter.

There were 139 distinct LULC change trajectories during 2000–2020. As Table 3 indicates, the predominant change type was the stable change type, followed by the late-stage change type, with the areas accounting for 86.96% and 10.86% of the total area, respectively. The stable change trajectory with the largest area was farmland-farmland-farmland, covering an area of 19,461.01 km^2, which accounted for 49.30% of the total stable change area. This is largely attributed to the significant proportion of farmland in the region. The most extensive early-stage change trajectory with the largest area was grassland-forest-forest, while the late-stage change trajectory with the largest area was grassland-grassland-farmland. The repeated change trajectory with the largest area was farmland-grassland-farmland. The area of the continuous change type accounted for the smallest proportion of the total area, but the change trajectory varied the most.

Table 3 Number of trajectories, areas, and area proportions of different LULC change types, along with the areas and area proportions of different LULC change trajectories (with the largest area) in the period 2000–2020

LULC change type	Number of trajectories	Area (km^2)	Area proportion of the total area (%)	LULC change trajectory with the largest area	Area (km^2)	Area proportion of the type area (%)
Stable change	6	39471.99	86.96	Farmland-farmland-farmland	19,461.01	49.30
Early-stage change	21	696.31	1.53	Grassland-forest-forest	311.64	44.76
Late-stage change	28	4931.23	10.86	Grassland-grassland-farmland	1213.98	24.62
Repeated change	21	224.26	0.49	Farmland-grassland-farmland	45.60	20.33
Continuous change	63	67.03	0.15	Grassland-forest-farmland	20.64	30.79

In summary, Table 3 reveals that the most extensive change trajectories involved transitions among farmland, grassland, and forest. This is primarily due to the substantial area these LULC types occupied in the JRB. Besides the stable change type, the area of the late-stage change type occupied the largest proportion of the total area (83.31%), suggesting more active LULC changes during 2010–2020. The predominant late-stage change trajectory, grassland-grassland-farmland, corroborated the considerable exchange between farmland and grassland observed in Figure 5. Excluding the stable change type, Table 4 lists the first ten LULC change trajectories in the period 2000–2020.

Table 4 Description of the first ten LULC change trajectories in the period 2000–2020

Number	Change trajectory	Change type	Area (km^2)	Transfer rate (%)	Cumulative transfer rate (%)
1	Grassland-grassland-farmland	Late-stage change	1213.98	20.51	20.51
2	Farmland-farmland-grassland	Late-stage change	1152.00	19.46	39.97
3	Forest-forest-grassland	Late-stage change	706.26	11.93	51.91
4	Grassland-grassland-forest	Late-stage change	655.67	11.08	62.98
5	Farmland-farmland-urban land	Late-stage change	573.37	9.69	72.67
6	Grassland-forest-forest	Early-stage change	311.64	5.27	77.94
7	Farmland-farmland-forest	Late-stage change	267.78	4.52	82.46
8	Grassland-grassland-farmland	Late-stage change	196.05	3.31	85.77
9	Farmland-urban land-urban land	Early-stage change	102.46	1.73	87.50
10	Water body-farmland-farmland	Early-stage change	68.08	1.15	88.65

Excluding the stable change type, there were 133 LULC change trajectories in the JRB during 2000–2020. Table 4 shows that the cumulative transfer rate of the first ten LULC change trajectories reached 88.65%. Of these, three change trajectories were classified as the early-stage change type, while seven were categorized as the late-stage change type. These trajectories primarily highlighted the mutual conversions among farmland, forest, and grassland, followed by the transitions from farmland to urban land and from water body to farmland. A comparative analysis of Table 4 and Figure 4 reveals that grassland had the highest transfer rate, followed by farmland, for both two- and three-time-node periods. Specifically, the transfer rate was 35.99% from grassland to forest in the period 2000–2010, 24.17% from grassland to farmland in the period 2010–2020, and 20.51% for the change trajectory of grassland-grassland-farmland over the entire period from 2000 to 2020.

3.2 Spatial characteristics of LULC change trajectories

Analysis of Figure 5 reveals that the exchanges of farmland and urban land between 2000 and 2010, and those of farmland, forest, and grassland during 2010–2020, were more pronounced than the net changes. This suggests significant spatial changes in these LULC types. Standard deviation ellipses were utilized to further explore the spatial characteristics of LULC changes. LULC change categories in the periods 2000–2010 and 2010–2020 were extracted, and the corresponding standard deviation ellipses were generated using tools in ArcGIS, as illustrated in Figure 7.

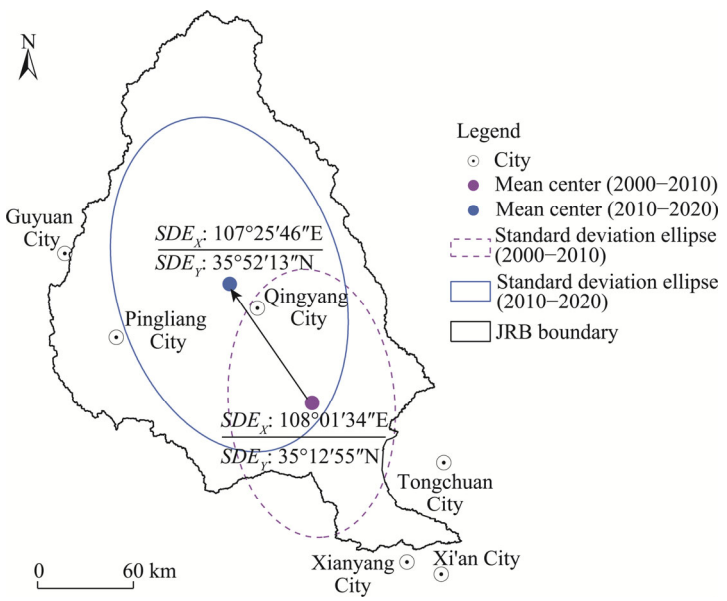

Fig. 7 Spatial variations in the standard deviation ellipses of LULC changes and their mean centers from the period 2000–2010 to the period 2010–2020 in the JRB. *SDEX* and *SDEY* represent the spatial coordinates of the mean center of the standard deviation ellipse along the *X* and *Y* axes, respectively.

The mean center was located at 108°01′34″E and 35°12′55″N during 2000–2010, and shifted to 107°25′46″E and 35°52′13″N during 2010–2020. This shift indicates a northwestward movement of the LULC change center (from the border of Shaanxi Province to Gansu Province), over the two decades. Table 5 details the parameters of the standard deviation ellipses in the periods 2000–2010 and 2010–2020. It is evident that the area and perimeter of the standard deviation ellipse in the period 2000–2010 were smaller than those in the period 2010–2020 (Fig. 7; Table 5). During 2000–2010, the difference between the lengths of the long and short axes was 32.10 km, with a short-to-long axis ratio of 0.62. In contrast, in the period 2010–2020, this difference increased to 36.25 km, and the ratio rose to 0.66. These differences suggest that during 2000–2010, LULC

changes were more cohesive in the JRB, while during 2010–2020, LULC changes were more spatially dispersed and less directionally oriented.

Table 5 reveals that in the period 2000–2010, both the short and long axes of the standard deviation ellipse were shorter than those in the period 2010–2020. This suggests that the spatial concentration of LULC changes was more pronounced in the earlier period, while the range of changes expanded significantly in the later period. The increases in the lengths of the short and long axes indicate that LULC changes in the JRB extended in both east-west and north-south directions from 2000 to 2020. The azimuth angle decreased from 175.41° to 163.71° during these two periods. Initially, LULC changes were primarily concentrated in Shaanxi Province and Gansu Province during 2000–2010, expanding into Ningxia Hui Autonomous Region during 2010–2020. Overall, LULC changes in the JRB from 2000 to 2020 exhibited a discrete expansion trend, with a more pronounced change pattern and a general southeast to northwest directional shift.

Table 5 Parameters of the standard deviation ellipses of LULC changes in the periods 2000–2010 and 2010–2020

Study period	Long axis length (km)	Short axis length (km)	Area (km^2)	Perimeter (km)	Azimuth angle (°)
2000–2010	84.28	52.18	13,813.60	434.63	175.41
2010–2020	107.29	71.04	23,942.30	566.03	163.71

3.3 Driving factors of the spatial differentiation of LULC changes

3.3.1 Factor detector analysis

The factor detector was utilized to assess the influence of individual driving factors on the spatial differentiation of LULC changes during 2000–2010 and 2010–2020, as shown in Figure 8.

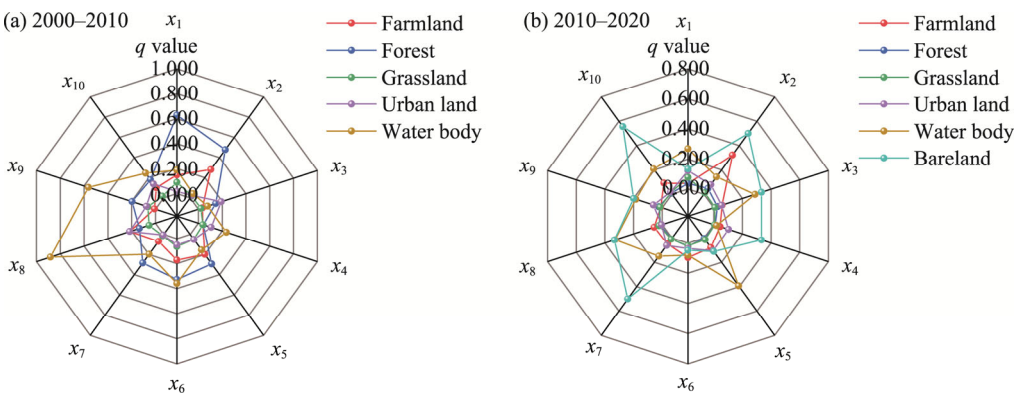

Fig. 8 Factor detector results (indicated by the q values) showing the influence of individual driving factors on the spatial differentiation of LULC changes in the JRB during 2000–2010 (a) and 2010–2020 (b). x_1 to x_{10} corresponded to DEM, slope, aspect, curvature, GDP, population, distance from railways, distance from highways, distance from water, and distance from residents, respectively. q is the explanatory power of driving factors on the spatial differentiation of LULC changes.

Figure 8 shows that during 2000–2010, slope and DEM were the significant natural factors influencing the spatial differentiation of farmland and forest changes, while distance from highways influenced urban land and water body. In the period 2010–2020, DEM and slope continued to be influential, along with GDP and distance from residents. Specifically, the spatial differentiation patterns of water body, forest, and farmland changes were significantly affected by distance from highways, DEM, and DEM, respectively, with q values of 0.883, 0.629, and 0.281, respectively. During 2010–2020, the spatial differentiation patterns of bareland, water body, and farmland changes were most influenced by distance from residents, GDP, and DEM, respectively (q values of 0.556, 0.393, and 0.323, respectively). Since bareland did not change during

2000–2010, a factor detector analysis was not conducted.

Factor detector analysis indicates that while natural and accessibility factors were predominant in influencing LULC changes from 2000 to 2010, the role of socio-economic factors became more pronounced during 2010–2020. This trend suggests that LULC changes in the JRB were increasingly driven by a combination of diverse factors, including the growing impact of socio-economic development. Notably, water body, bareland, forest, and farmland were significantly affected by individual factors throughout the entire period from 2000 to 2020, with water body being particularly influenced. In summary, LULC changes in the JRB were primarily driven by natural factors, but with the development of the social economy, the influences of human activities on these changes have become increasingly significant (Zhang et al., 2022).

3.3.2 Interaction detector analysis

Building on the results from the factor detector analysis, the interaction detector was employed to examine the combined effect of two driving factors on the spatial differentiation of LULC changes in the JRB during the periods 2000–2010 and 2010–2020 (Figs. 9 and 10).

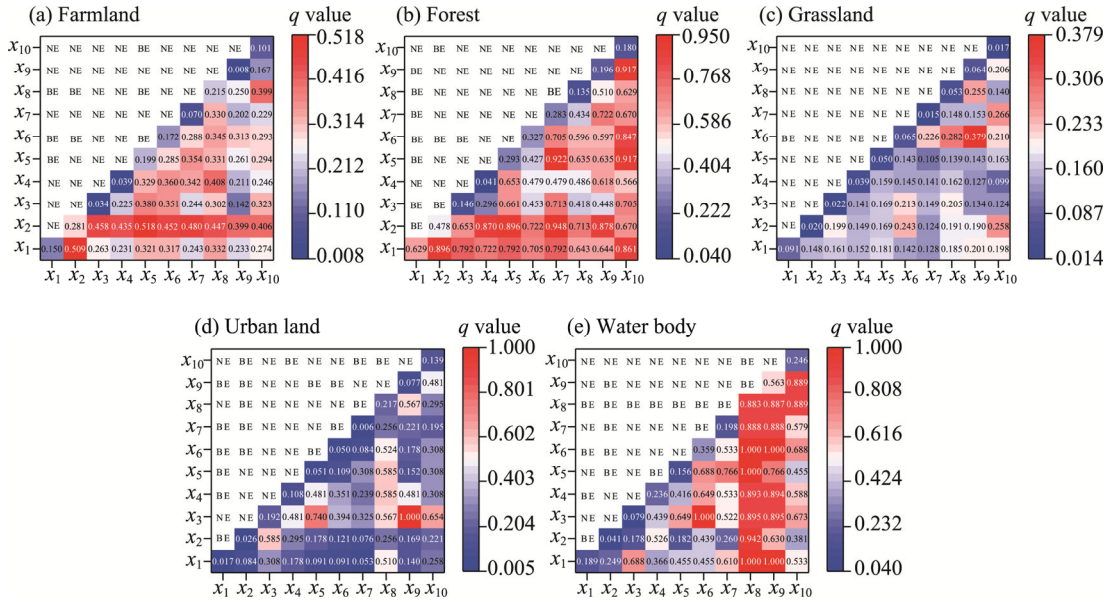

Fig. 9 Interaction detector results and q values for various driving factors influencing the spatial differentiation of farmland (a), forest (b), grassland (c), urban land (d), and water body (e) changes in the JRB in the period 2000–2010. x_1 to x_{10} denoted DEM, slope, aspect, curvature, GDP, population, distance from railways, distance from highways, distance from water, and distance from residents, respectively. NE, nonlinear enhancement; BE, bilinear enhancement.

Figure 9 indicates that the interactions among driving factors predominantly resulted in bilinear or nonlinear enhancement on influencing the spatial differentiation of LULC changes in the JRB during 2000–2010. This suggests that LULC changes were influenced by a combination of multiple driving factors. Specifically, the interactions between slope and other factors notably impacted the spatial differentiation of farmland changes, with the combination of DEM and slope exerting the greatest influence (q value of 0.509; Fig. 9a). Figure 9b illustrates that the interactions among DEM, slope, GDP, and distance from residents significantly influenced the spatial differentiation of forest changes. Notably, the interaction of slope with distance from railways was the most influential on forest, with a q value of 0.948. Figure 9c reveals that the interactions among driving factors had minimal impact on the spatial differentiation of grassland changes during 2000–2010. In Figure 9d, aspect, in combination with other factors, strongly affected the spatial differentiation of urban land changes. As shown in Figure 9e, the interactions between distance from highways and other factors, including DEM, GDP, and population, as well

as between distance from water and other factors, significantly influenced the spatial differentiation of water body changes, some reaching the extreme states of interaction. Since bareland did not change during 2000–2010, an interaction detector analysis was not conducted.

Figure 10 presents the interaction detector results for LULC changes in the JRB during 2010–2020, showing predominantly bilinear or nonlinear enhancement. These results suggest that the spatial differentiation of LULC changes were influenced by a combination of multiple driving factors. Specifically, the interactions between slope and other factors significantly impacted the spatial differentiation of farmland changes, with the combination of population and slope exerting the greatest influence (q value of 0.413; Fig. 10a). The interactions among driving factors had minimal impact on the spatial differentiation of forest and grassland changes during this period (Fig. 10b and c). The spatial differentiation of urban land changes was significantly affected by the interactions of slope, aspect, and other factors (Fig. 10d). The interactions of aspect and distance from highways, along with other factors, had a strong influence on the spatial differentiation of water body changes (Fig. 10e). Notably, the combinations of aspect with slope and GDP, as well as the interaction between distance from highways and GDP, were particularly influential, with q values of 0.966, 0.820, and 0.798, respectively. The spatial differentiation of bareland changes was greatly affected by the interactions of slope, GDP, distance from railways, distance from highways, distance from water, and distance from residents during this period (Fig. 10f).

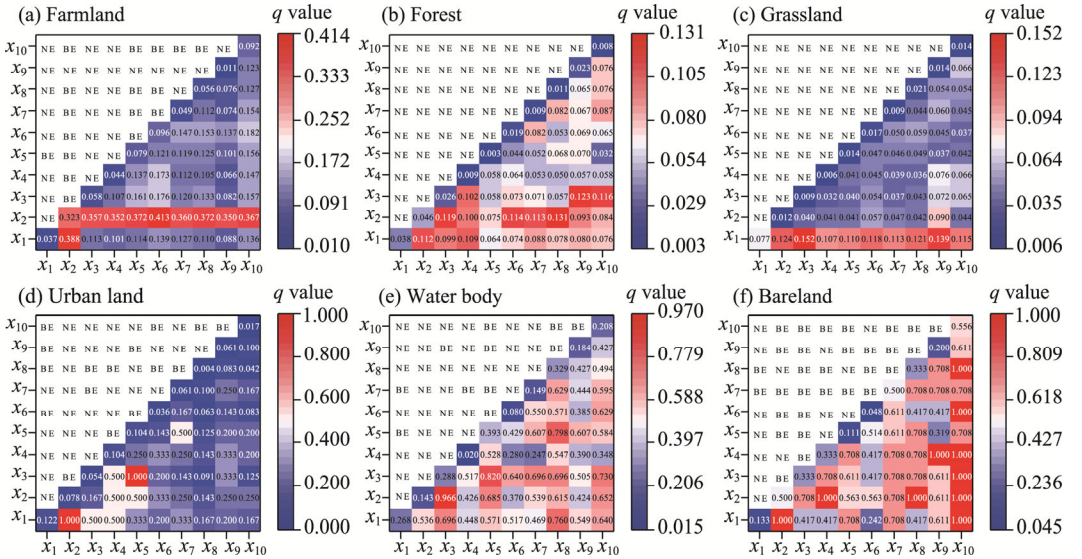

Fig. 10 Interaction detector results and q values for various driving factors influencing the spatial differentiation of farmland (a), forest (b), grassland (c), urban land (d), water body (e), and bareland (f) changes in the JRB in the period 2010–2020. x_1 to x_{10} corresponded to DEM, slope, aspect, curvature, GDP, population, distance from railways, distance from highways, distance from water, and distance from residents, respectively. NE, nonlinear enhancement; BE, bilinear enhancement.

Synthesizing the findings from Figures 9 and 10, it is evident that the interactions between slope and other factors had significant influences on the spatial differentiation of farmland changes throughout the period 2000–2020. This is likely because slope directly reflects topographical conditions, affecting the quality of farmland. For the spatial differentiation of forest changes, the influence of driving factors was more pronounced during 2000–2010, possibly due to the comprehensive implementation of the "Grain for Green Project" in this period. The interactions of driving factors had no significant effect on the spatial differentiation of grassland changes over the two decades. For urban land, the interactions of aspect with other factors, especially aspect and GDP (with q values exceeding 0.700), were influential during both periods (2000–2010 and 2010–2020). The spatial differentiation of water body changes was greatly affected by the interactions between distance from highways and other factors, especially the

combination with GDP. For bareland, there were no significant influences from the interactions of driving factors during 2000–2010, but the interactions between accessibility factors and other driving factors became more evident during 2010–2020.

4 Discussion

The LULC change trajectory analysis method effectively captures the dynamic changes of LULC for each grid at different time nodes. This study extended the analysis by integrating the Geodetector model to investigate the driving factors of LULC changes. While previous research has focused on the impacts of LULC changes on hydrological processes (Jiang et al., 2015; Ji and Duan, 2019) and ecological environment (Wu et al., 2022a; Xu et al., 2022b), there has been limited quantitative analysis on the driving factors of LULC changes in the JRB. This paper calculated the net change, exchange, total change, and transfer rate of LULC types in the JRB during 2000–2020. Through the LULC change trajectory analysis, knowledge maps, chord diagrams, and standard deviation ellipse method, we analyzed the spatiotemporal characteristics of LULC changes in the JRB from 2000 to 2020. The factor detector and interaction detector in the Geodetector model were utilized to explore the driving mechanisms of LULC changes, highlighting the influence of individual factors and their combined effect on the spatial differentiation of LULC changes, as reflected by the q values.

From 2000 to 2020, LULC changes in the JRB predominantly involved the conversions of farmland, forest, and grassland. This is not only due to their large joint area, but also because of the "Grain for Green Project". Since 1999, increased measures under this project, such as closing mountains and grazing prohibition (Huang et al., 2021), have been implemented in the JRB and its surrounding areas. However, as revealed in Section 3.1, the changes among farmland, forest, and grassland were not merely a reduction in the areas of farmland and grassland with a corresponding increase in the area of forest. Rather, they represented complex transformations among these types, largely due to the "Grain for Green Project" that requires afforestation and the restoration and transformation of degraded grassland (Xu et al., 2022b). The expansion in urban land was primarily attributed to the conversion of farmland, associated with urban sprawl. LULC changes were more pronounced during 2010–2020 compared to the period 2000–2010, likely because the benefits of reforestation and grassland restoration projects became more visible after 2010 (Xu et al., 2022a; Yu et al., 2023). Consequently, the entire basin shifted towards a medium-high vegetation cover level, leading to increased vegetation cover and more evident LULC changes (Zhang et al., 2022).

LULC changes in the JRB from 2000 to 2020 involved not only quantitative alterations but also significant spatial shifts. Specifically, during 2000–2010, the primary quantitative changes occurred in forest, whereas, in the period 2010–2020, farmland and grassland experienced more pronounced changes (as illustrated in Figs. 4 and 6). The mean center of the standard deviation ellipse of LULC changes was situated in the downstream of the JRB during 2000–2010, shifting to the midstream and upstream regions in the following decade (Fig. 7). This observation was corroborated by Xu et al. (2022a), who noted that from 2000 to 2020, changes in farmland predominantly occurred in the upstream of the JRB, while forest changes were more concentrated in the downstream region, and grassland changes were mainly in the midstream and upstream areas. LULC changes exhibited a discrete expansion trend from southeast to northwest across the JRB during this period (Fig. 7), aligning with the spatial variation trend of the coefficient of variation of the NDVI increasing from southeast to northwest (Xu et al., 2022a). This trend suggests that LULC changes were largely characterized by the transformations among farmland, forest, and grassland, which are key indicators of vegetation coverage. The greater variability in NDVI indicates a more dispersed vegetation distribution. NDVI decreased from southeast to northwest in the JRB (Lyu et al., 2023), mirroring the shift in the mean center of the standard deviation ellipse of LULC changes from southeast during 2000–2010 to northwest during 2010–2020. This implies that LULC changes were more pronounced in areas with lower

vegetation coverage. However, vegetation coverage in the upstream areas still requires enhancement (Xu and Pan, 2022), a need that is closely tied to local policies focusing on vegetation restoration and soil and water conservation.

Slope, as a natural factor, along with GDP being a socio-economic factor and distance from highways being an accessibility factor, emerged as the primary drivers of the spatial differentiation of LULC changes in the JRB during 2000–2020. Factor detector results indicate that slope predominantly influenced the spatial differentiation of farmland changes, whereas GDP and distance from highways mainly affected the spatial differentiation of water body changes (Fig. 9). Interaction detector findings reveal that the spatial differentiation of farmland changes was largely influenced by the interaction between slope and DEM (Fig. 10). Wang et al. (2018) have previously acknowledged the significant impact of slope and DEM on the spatiotemporal characteristics of regional LULC. The spatial differentiation of urban land changes were primarily driven by the interplay between aspect and GDP, resonating with the findings that economic factors significantly drive the conversion of farmland to urban land (Alijani et al., 2020). This suggests that GDP, as a key socioeconomic factor, may propel the transformation of farmland to urban land. The spatial differentiation of water body changes was notably influenced by the interaction between distance from highways and GDP, supporting the study of Han et al. (2021) using highway proximity as a measure of human activities impacting LULC changes. Our results align with the notion that LULC changes occur more likely near the highways and are significantly affected by human activities, as also highlighted by Alijani et al. (2020).

The interaction type of two driving factors influencing the LULC changes in the JRB was predominantly characterized as nonlinear or bilinear enhancement during 2000–2020. This underscores that a multifaceted consideration of various driving factors and their interactions can elucidate the driving mechanisms of LULC changes more effectively than any single factor. Zhang et al. (2022) arrived at a similar conclusion in their study on the ecological index of the Weihe River Basin, China, illustrating that the mechanisms of LULC changes are responsive to the ecological environment. This emphasizes the importance of investigating the LULC change drivers in the context of a changing environment. Future studies should delve deeper into the synergistic effects among driving factors, such as the interactions between aspect and GDP and between distance from highways and GDP, to more comprehensively understand how these factors influence LULC changes amidst environmental uncertainties.

While this study combined change trajectory analysis with the Geodetector model and incorporated multiple driving factors to explore the spatiotemporal characteristics and driving mechanisms of LULC changes in the JRB, there are inherent limitations due to data availability. For instance, the use of LULC data in only 2000, 2010, and 2020 precluded a more detailed yearly analysis of LULC changes. Nevertheless, our key findings regarding LULC changes in the JRB during 2000–2020 align with those of Wu et al. (2022b), Xu et al. (2022b), and Zhang et al. (2022). In terms of driving factors, climate variables such as precipitation and temperature were not included in this study, given the subsequent special focus on the impacts of historical and future climate change on LULC, as well as their combined effect on the ecological environment of the JRB.

5 Conclusions

Utilizing LULC data in 2000, 2010, and 2020, this paper computed the net change, exchange, total change, and transfer rate of LULC in the JRB. The spatiotemporal characteristics of LULC changes during 2000–2020 were thoroughly examined by employing methods such as LULC change trajectory analysis, knowledge maps, chord diagrams, and standard deviation ellipses. The study also identified driving factors in natural, socio-economic, and accessibility domains and analyzed their impacts on the spatial differentiation of LULC changes using factor detector and interaction detector in the Geodetector model. The key findings are as follows:

(1) From 2000 to 2020, LULC changes in the JRB were primarily characterized by the

transformations among farmland, forest, and grassland. These changes were complex and dynamic, heavily influenced by the ecological and environmental protection policies, such as the "Grain for Green Project". Excluding the stable change type, the majority of LULC changes were classified as the late-stage change type, with the areas accounting for 10.86% of the total area and 83.31% of the total change area. LULC knowledge maps and chord diagrams reveal that LULC changes were more active and intricate during 2010–2020 compared to the period 2000–2010, indicating a heightened disturbance from human activities in the latter decade. LULC changes exhibited a discrete spatial expansion trend from 2000 to 2020. The scope of changes extended from Shaanxi Province and Gansu Province to the Ningxia Hui Autonomous Region. The general direction of LULC changes was from southeast to northwest in the JRB.

(2) A thorough evaluation of the results from the factor detector and interaction detector reveals significant insights into LULC changes in the JRB. Changes in water body and bareland were considerably impacted by both single driving factor and interactional driving factors. Forest and farmland changes were primarily influenced by single driving factor. In contrast, grassland changes were less affected by either single driving factor or interactional driving factors. Urban land changes, however, were notably affected by interactional driving factors. During 2000–2020, LULC changes in the JRB were chiefly characterized by bilinear or nonlinear enhancement. Slope (as a natural factor), GDP (as a socio-economic factor), and distance from highways (as an accessibility factor) emerged as significant drivers in influencing LULC changes throughout the two periods. Notably, the impact of socio-economic factors on LULC changes increased from 2010 to 2020.

The insights derived from this research provide a valuable scientific basis for the rational management and sustainable development of LULC under the evolving environmental conditions in the JRB.

Conflict of interest

The authors declare that they have no known competing financial interests or personal relationships that could have appeared to influence the work reported in this paper.

Acknowledgements

The study was partly funded by the National Key Research and Development Program of China (NK2023190801), the National Foreign Experts Program of China (G2023041024L), and the Key Scientific Research Program of Shaanxi Provincial Education Department, China (21JT028). We sincerely appreciate the editors and anonymous reviewers for their help in improving the article.

Author contributions

Conceptualization: WANG Yinping, JIANG Rengui; Data curation: WANG Yinping; Methodology: WANG Yinping; Writing - original draft preparation: WANG Yinping; Writing - review and editing: WANG Yinping, JIANG Rengui; Funding acquisition: JIANG Rengui, XIE Jiancang; Resources: JIANG Rengui, XIE Jiancang, ZHAO Yong; Supervision: YANG Mingxiang, LI Fawen, LU Xixi. All authors approved the manuscript.

References

Alijani Z, Hosseinali F, Biswas A. 2020. Spatio-temporal evolution of agricultural land use change drivers: A case study from Chalous region, Iran. Journal of Environment Management, 262: 110326, doi: 10.1016/j.jenvman.2020.110326.

Asenso Barnieh B, Jia L, Menenti M, et al. 2022. Quantifying spatial reallocation of land use/land cover categories in West Africa. Ecology Indicators, 135: 108556, doi: 10.1016/j.ecolind.2022.108556.

Chen Q, Bi Y Z, Li J F. 2021. Spatial disparity and influencing factors of coupling coordination development of economy-environment-tourism-traffic: A case study in the middle reaches of Yangtze River urban agglomerations. International Journal of Environmental Research and Public Health, 18(15): 7947, doi: 10.3390/ijerph18157947.

Dong S W, Chen Z Y, Gao B B, et al. 2020. Stratified even sampling method for accuracy assessment of land use/land cover

classification: A case study of Beijing, China. International Journal of Remote Sensing, 41(16): 6427–6443.

Gong W F, Duan X Y, Mao M J, et al. 2022. Assessing the impact of land use and changes in land cover related to carbon storage by linking trajectory analysis and InVEST models in the Nandu River Basin on Hainan Island in China. Frontiers in Environmental Science, 10: 1038752, doi: 10.3389/fenvs.2022.1038752.

Han J J, Wang J P, Chen L, et al. 2021. Driving factors of desertification in Qaidam Basin, China: An 18-year analysis using the geographic detector model. Ecology Indicators, 124: 107404, doi: 10.1016/j.ecolind.2021.107404.

He Q Q, Meng Q, Flatley W, et al. 2022. Examining the effects of agricultural aid on forests in sub-Saharan Africa: A causal analysis based on remotely sensed data of Sierra Leone. Land, 11(5): 668, doi: 10.3390/land11050668.

Heidarlou H B, Shafiei A B, Erfanian M, et al. 2020. Underlying driving forces of forest cover changes due to the implementation of preservation policies in Iranian northern Zagros forests. International Forestry Review, 22(2): 241–256.

Helbich M, Yao Y, Liu Y, et al. 2019. Using deep learning to examine street view green and blue spaces and their associations with geriatric depression in Beijing, China. Environment International, 126: 107–117.

Huang C L, Yang Q K, Huang W D. 2021. Analysis of the spatial and temporal changes of NDVI and its driving factors in the Wei and Jing River basins. International Journal of Environmental Research and Public Health, 18(22): 11863, doi: 10.3390/ijerph182211863.

Ji L, Duan K Q. 2019. What is the main driving force of hydrological cycle variations in the semiarid and semi-humid Weihe River Basin, China? Science of the Total Environment, 684: 254–264.

Ji X L, Sun Y L, Guo W, et al. 2023. Land use and habitat quality change in the Yellow River Basin: A perspective with different CMIP6-based scenarios and multiple scales. Journal of Environmental Management, 345: 118729, doi: 10.1016/j.jenvman.2023.118729.

Jiang C, Xiong L H, Wang D B, et al. 2015. Separating the impacts of climate change and human activities on runoff using the Budyko-type equations with time-varying parameters. Journal of Hydrology, 522: 326–338.

Jiang R G, Wang Y P, Xie J C, et al. 2019. Assessment of extreme precipitation events and their teleconnections to El Nino Southern Oscillation, a case study in the Wei River Basin of China. Atmosphere Research, 218: 372–384.

Kayitesi N M, Guzha A C, Mariethoz G. 2022. Impacts of land use land cover change and climate change on river hydro-morphology—a review of research studies in tropical regions. Journal of Hydrology, 615: 128702, doi: 10.1016/j.jhydrol.2022.128702.

Lefever D W. 1926. Measuring geographic concentration by means of the standard deviational ellipse. American Journal of Sociology, 32(1): 88–94.

Li J, Jiang Z, Miao H, et al. 2022. Identification of cultivated land change trajectory and analysis of its process characteristics using time-series Landsat images: A study in the overlapping areas of crop and mineral production in Yanzhou City, China. Science of the Total Environment, 806: 150318, doi: 10.1016/j.scitotenv.2021.150318.

Liu S L, Dong Y H, Wang F F, et al. 2022. Priority area identification of ecological restoration based on land use trajectory approach—Case study in a typical karst watershed. Frontiers in Environmental Science, 10: 1011755, doi: 10.3389/fenvs.2022.1011755.

Luo J, Xin L J, Liu F G, et al. 2022. Study of the intensity and driving factors of land use/cover change in the Yarlung Zangbo River, Nyang Qu River, and Lhasa River region, Qinghai-Tibet Plateau of China. Journal of Arid Land, 14(4): 411–425.

Lyu J Q, Yin S S, Sun Y T, et al. 2023. Flood runoff simulation under changing environment, based on multiple satellite data in the Jinghe River Basin of the Loess Plateau, China. Remote Sensing, 15(3): 550, doi: 10.3390/rs15030550.

Niu H P, Zhao X M, Xiao D Y, et al. 2022. Evolution and influencing factors of landscape pattern in the Yellow River Basin (Henan Section) due to land use changes. Water, 14(23): 3872, doi: 10.3390/w14233872.

Schirpke U, Tasser E, Borsky S, et al. 2023. Past and future impacts of land-use changes on ecosystem services in Austria. Journal of Environmental Management, 345: 118728, doi: 10.1016/j.jenvman.2023.118728.

Wang D C, Gong J H, Chen L D, et al. 2012. Spatio-temporal pattern analysis of land use/cover change trajectories in Xihe watershed. International Journal of Applied Earth Observation and Geoinformation, 14(1): 12–21.

Wang D C, Sang M Q, Huang Y, et al. 2019a. Trajectory analysis of agricultural lands occupation and its decoupling relationships with the growth rate of non-agricultural GDP in the Jing-Jin-Tang region, China. Environment Development and Sustainability, 21(2): 799–815.

Wang H, Liu G H, Li Z S, et al. 2018. Assessing the driving forces in vegetation dynamics using net primary productivity as the indicator: A case study in Jinghe River Basin in the Loess Plateau. Forests, 9(7): 374, doi: 10.3390/f9070374.

Wang J F, Li X H, Christakos G, et al. 2010. Geographical detectors-based health risk assessment and its application in the neural tube defects study of the Heshun Region, China. International Journal of Geographical Information Science, 24(1): 107–127.

Wang S, Zhang Q, Yang T, et al. 2019b. River health assessment: Proposing a comprehensive model based on physical habitat, chemical condition and biotic structure. Ecology Indicators, 103: 446–460.

Wang X J, Liu G X, Xiang A C, et al. 2023. Terrain gradient response of landscape ecological environment to land use and land cover change in the hilly watershed in South China. Ecology Indicators, 146: 109797, doi: 10.1016/j.ecolind.2022.109797.

Wang Y P, Jiang R G, Xie J C, et al. 2019c. Soil and Water Assessment Tool (SWAT) model: A systemic review. Journal of Coastal Research, 93(SI): 22–30.

Wang Y P, Jiang R G, Xie J C, et al. 2022. Bias correction, historical evaluations, and future projections of climate simulations in the Wei River Basin using CORDEX-EA. Theoretical and Applied Climatology, 150(1–2): 135–153.

Wu C X, Qiu D X, Gao P, et al. 2022a. Application of the InVEST model for assessing water yield and its response to precipitation and land use in the Weihe River Basin, China. Journal of Arid Land, 14(4): 426–440.

Wu J Y, Luo J G, Zhang H, et al. 2022b. Projections of land use change and habitat quality assessment by coupling climate change and development patterns. Science of the Total Environment, 847: 157491, doi: 10.1016/j.scitotenv.2022.157491.

Xia N, Hai W Y, Tang M Y, et al. 2023. Spatiotemporal evolution law and driving mechanism of production-living-ecological space from 2000 to 2020 in Xinjiang, China. Ecology Indicators, 154: 110807, doi: 10.1016/j.ecolind.2023.110807.

Xu B, Qi B, Ji K, et al. 2022a. Emerging hot spot analysis and the spatial-temporal trends of NDVI in the Jing River Basin of China. Environmental Earth Sciences, 81(2): 55, doi: 10.1007/s12665-022-10175-5.

Xu B C, Pan J H. 2022. Simulation and measurement of soil conservation service flow in the Loess Plateau: A case study for the Jinghe River Basin, Northwestern China. Ecological Indicators, 141: 109072, doi: 10.1016/j.ecolind.2022.109072.

Xu C, Jiang Y N, Su Z H, et al. 2022b. Assessing the impacts of Grain-for-Green Programme on ecosystem services in Jinghe River basin, China. Ecology Indicators, 137: 108757, doi: 10.1016/j.ecolind.2022.108757.

Xu D, Hou G L. 2019. The spatiotemporal coupling characteristics of regional urbanization and its influencing factors: Taking the Yangtze River Delta as an example. Sustainability, 11(3): 822, doi: 10.3390/su11030822.

Yang H F, Zhong X N, Deng S Q, et al. 2022. Impact of LUCC on landscape pattern in the Yangtze River Basin during 2001–2019. Ecological Informatics, 69: 101631, doi: 10.1016/j.ecoinf.2022.101631.

Yang J, Xie B P, Zhang D G, et al. 2021. Climate and land use change impacts on water yield ecosystem service in the Yellow River Basin, China. Environmental Earth Sciences, 80(3): 72, doi: 10.1007/s12665-020-09277-9.

Yu Y P, Yu P T, Wang Y H, et al. 2023. Natural revegetation has dominated annual runoff reduction since the Grain for Green Program began in the Jing River Basin, Northwest China. Journal of Hydrology, 625: 129978, doi: 10.1016/j.jhydrol.2023.129978.

Zhai H, Lv C Q, Liu W Z, et al. 2021. Understanding spatio-temporal patterns of land use/land cover change under urbanization in Wuhan, China, 2000–2019. Remote Sensing, 13(16): 3331, doi: 10.3390/rs13163331.

Zhan D S, Kwan M P, Zhang W Z, et al. 2018. The driving factors of air quality index in China. Journal of Cleaner Production, 197: 1342–1351.

Zhang K L, Feng R R, Zhang Z C, et al. 2022. Exploring the driving factors of remote sensing ecological index changes from the perspective of geospatial differentiation: A case study of the Weihe River Basin, China. International Journal of Environmental Research and Public Health, 19(17): 10930, doi: 10.3390/ijerph191710930.

Zhang Z, Hu B Q, Jiang W G, et al. 2021. Identification and scenario prediction of degree of wetland damage in Guangxi based on the CA-Markov model. Ecology Indicators, 127: 107764, doi: 10.1016/j.ecolind.2021.107764.

Zhao Z Z, Tang X J, Wang C, et al. 2023. Analysis of the spatial and temporal evolution of the GDP in Henan Province based on nighttime light data. Remote Sensing, 15(3): 716, doi: 10.3390/rs15030716.

Zhou C S, Chen J, Wang S J. 2018. Examining the effects of socioeconomic development on fine particulate matter (PM2.5) in China's cities using spatial regression and the geographical detector technique. Science of the Total Environment, 619–620: 436–445.

Zhou Q M, Li B L, Kurban A. 2008. Spatial pattern analysis of land cover change trajectories in Tarim Basin, northwest China. International Journal of Remote Sensing, 29(19): 5495–5509.

Zhou X, Wu D, Li J F, et al. 2022. Cultivated land use efficiency and its driving factors in the Yellow River Basin, China. Ecology Indicators, 144: 109411, doi: 10.1016/j.ecolind.2022.109411.

Zhu Z Y, Dai Z Z, Li S L, et al. 2022. Spatiotemporal evolution of non-grain production of cultivated land and its underlying factors in China. International Journal of Environmental Research and Public Health, 19(13): 8210, doi: 10.3390/ijerph19138210.

Zomlot Z, Verbeiren B, Huysmans M, et al. 2017. Trajectory analysis of land use and land cover maps to improve spatial-temporal patterns, and impact assessment on groundwater recharge. Journal of Hydrology, 554: 558–569.